



A new data fusion model for high spatial- and temporal-resolution mapping of forest disturbance based on Landsat and MODIS

Thomas Hilker^{a,*}, Michael A. Wulder^b, Nicholas C. Coops^a, Julia Linke^c, Greg McDermid^c, Jeffrey G. Masek^d, Feng Gao^d, Joanne C. White^b

^a Integrated Remote Sensing Studio, Department of Forest Resource Management, University of British Columbia, 2424 Main Mall, University of British Columbia, Vancouver, British Columbia, Canada V6T 1Z4

^b Canadian Forest Service (Pacific Forestry Centre), Natural Resources Canada, Victoria, British Columbia, Canada V8Z 1M5

^c Foothills Facility for Remote Sensing and GI-Science, Department of Geography, University of Calgary, 2500 University Drive, NW, Calgary, Alberta, Canada T2N 1N4

^d Biospheric Sciences Branch, NASA Goddard Space Flight Center, Greenbelt MD, 20771, USA

ARTICLE INFO

Article history:

Received 30 January 2009

Received in revised form 10 March 2009

Accepted 14 March 2009

Keywords:

Landsat

MODIS

Change detection

Disturbance

Synthetic imagery

STARFM

STAARCH

Data blending

EOSD

ABSTRACT

Investigating the temporal and spatial pattern of landscape disturbances is an important requirement for modeling ecosystem characteristics, including understanding changes in the terrestrial carbon cycle or mapping the quality and abundance of wildlife habitats. Data from the Landsat series of satellites have been successfully applied to map a range of biophysical vegetation parameters at a 30 m spatial resolution; the Landsat 16 day revisit cycle, however, which is often extended due to cloud cover, can be a major obstacle for monitoring short term disturbances and changes in vegetation characteristics through time.

The development of data fusion techniques has helped to improve the temporal resolution of fine spatial resolution data by blending observations from sensors with differing spatial and temporal characteristics. This study introduces a new data fusion model for producing synthetic imagery and the detection of changes termed Spatial Temporal Adaptive Algorithm for mapping Reflectance Change (STAARCH). The algorithm is designed to detect changes in reflectance, denoting disturbance, using Tasseled Cap transformations of both Landsat TM/ETM and MODIS reflectance data. The algorithm has been tested over a 185 × 185 km study area in west-central Alberta, Canada. Results show that STAARCH was able to identify spatial and temporal changes in the landscape with a high level of detail. The spatial accuracy of the disturbed area was 93% when compared to the validation data set, while temporal changes in the landscape were correctly estimated for 87% to 89% of instances for the total disturbed area. The change sequence derived from STAARCH was also used to produce synthetic Landsat images for the study period for each available date of MODIS imagery. Comparison to existing Landsat observations showed that the change sequence derived from STAARCH helped to improve the prediction results when compared to previously published data fusion techniques.

© 2009 Elsevier Inc. All rights reserved.

1. Introduction

Natural and anthropogenic disturbances play a key role in terrestrial ecosystem functioning (Schimel et al., 1997; Hansen et al., 2001; Foster et al., 2003), and influence productivity and resource availability across a broad range of spatial and temporal dimensions. In forested environments, disturbance agents such as fire, insects, and various human activities related to settlement, cultivation, and resource extraction create pulses of biomass loss that influence biogeochemical cycling (DeFries et al., 1999; Patenaude et al., 2005; Morehouse et al., 2008; Masek & Collatz, 2006), and exert a strong imprint on both habitat structure (Mladenoff et al., 1993; Spies et al., 1994; Turner et al., 1997) and the distribution of wildlife species

(Foster et al., 2003; Nielsen et al., 2004; Linke et al., 2005; Lada et al., 2008; Leonard et al., 2008). As a result, detailed information on forest disturbance is important for a wide range of applications from ecological modeling to estimating carbon budgets on regional and global scales. Remote sensing is a critical data source for observing and understanding the effects of landscape disturbance (e.g. Potter et al., 2003; Linke et al., 2008; Masek et al., 2008), but trade-offs in sensor designs that balance spatial detail with concerns for swath width and repeat coverage (Price, 1994) can limit our capacity to monitor changes effectively (e.g. Gao et al., 2006; Pape & Franklin, 2008).

Landsat, with a spatial resolution of 30 m and spatial extent of 185 × 185 km per scene, is used widely for mapping biophysical vegetation parameters (Cohen & Goward, 2004; Masek et al., 2006) and has proven useful for monitoring land cover (Wulder et al., 2008; Linke et al., in press) and ecosystem disturbance (Healey et al., 2005; Masek et al., 2006; Masek et al., 2008). The minimum 16-day revisit cycle of the platform, however, which can be markedly extended due

* Corresponding author. Tel.: +1 604 822 4148; fax: +1 604 822 9106.

E-mail address: thilker@interchange.ubc.ca (T. Hilker).

to cloud contamination or duty cycle limitations (Ju & Roy, 2008) can create difficulties in capturing disturbance events in a timely manner (Gao et al., 2006; Leckie, 1990; Pape & Franklin, 2008). This can be a major concern, particularly in humid environments (Ranson et al., 2003; Roy et al., 2008; Ju & Roy, 2008), where the probability of acquiring cloud-free Landsat imagery for a given year (cloud cover <10%) can be as low as 10% (Leckie, 1990).

One technique for increasing the temporal frequency of high-spatial-resolution satellite observations is the blending of data from sensors with complementary spatial and temporal characteristics, with the aim of generating *synthetic* observations with both high spatial and temporal resolutions (Lunetta et al., 1998). For example, Gao et al. (2006) introduced the Spatial and Temporal Adaptive Reflectance Fusion Model (STARFM) to blend Landsat and Moderate Resolution Imaging Spectroradiometer (MODIS) data to generate synthetic Landsat-like imagery with a spatial resolution of 30 m on a daily basis. In another approach, Hansen et al. (2008) and Potapov et al. (2008) used regression trees to integrate Landsat and MODIS imagery to monitor deforestation in Africa and North America. A similar technique was also reported by Roy et al. (2008) for use in Landsat gap-filling and relative radiometric normalization procedures. Most data-fusion models use the high-spatial-resolution imagery to capture spatial details on the landscape, and incorporate the high-temporal-frequency data is used to describe changes over time. Previous research has shown this general approach to be successful for monitoring seasonal patterns in vegetation cover (Gao et al., 2006; Hilker et al., submitted for publication) and larger changes in land use (Hansen et al., 2008; Potapov et al., 2008). However, such data-fusion approaches are often based on spatially integrating reflectance observations and, as a result, are not specifically designed for mapping disturbance events, particularly if they occur in the sub-pixel range of the coarse-spatial-resolution image data.

Landsat-based detection of disturbances (e.g. Cohen et al., 2002; Franklin et al., 2001; Seto et al., 2002) commonly use image transformations such as the Tasseled Cap transformation (Crist & Cicone, 1984; Kauth & Thomas, 1976) to consolidate multispectral reflectance measurements and enhance the detection of disturbance events. The Tasseled Cap transformation reduces the Landsat reflectance bands to three orthogonal indices called brightness, greenness and wetness, and is a standard technique for describing the three major axes of spectral variation across the solar reflective spectrum measured by Landsat (Kauth & Thomas, 1976). Once an image is transformed into its Tasseled Cap data spaces, image arithmetic and thresholding techniques can be used to automatically identify and classify land cover changes and land cover disturbance (e.g. Cohen et al., 2002; Franklin et al., 2001; Healey et al., 2005).

While the 30-m spatial resolution of Landsat makes this data source highly suitable for detecting and delineating common disturbance events on the landscape (Masek et al., 2008; Wulder et al., 2004), the daily global revisit rate of MODIS offers attractive temporal capabilities. Although the Tasseled Cap transformation was originally developed for early Landsat sensors (multispectral scanner and thematic mapper) (Crist & Kauth, 1986; Crist & Cicone, 1984; Kauth & Thomas, 1976), its linear coefficients have more recently been modified for applicability to Enhanced Thematic Mapper Plus (ETM+) imagery and the MODIS land bands (Zhang et al., 2002). As a result, it is also possible to use Tasseled Cap transformation-based techniques on MODIS imagery to detect landscape disturbance at higher temporal resolutions. A data fusion approach can therefore be designed to capture high resolution spatial changes from Tasseled Cap Landsat observations, while the high frequency of MODIS observations can be used to accurately determine the time at which a given disturbance occurred.

In this study, we propose and validate a new spatially- and temporally-adaptive data fusion model for detection of disturbance and reflectance changes. The Spatial Temporal Adaptive Algorithm for mapping Reflectance Change (STAARCH) is based on a small number

(two or greater) of Landsat images and a temporally dense stack of spatially coincident MODIS imagery. The algorithm yields both a spatial change mask (derived from Landsat) and an image sequence which records the temporal evolution of disturbance events (derived from MODIS). STAARCH also includes functionality for estimating surface reflectance, based on an extended version of STARFM (Gao et al., 2006). We first develop the theoretical basis of STAARCH, and then demonstrate its application over a 185 × 185 km study area in west-central Alberta, Canada. Results were compared to a validation disturbance dataset which specifies the location and timing of anthropogenic and natural disturbance entities occurring in the study area between 2002 and 2005. Finally, we also compared estimated surface reflectance generated by STAARCH with Landsat observations collected in 2004.

2. Approach

2.1. Algorithm inputs and processing steps

In Fig. 1 we present an overview of the processing steps implemented in STAARCH, which are described in detail below. The algorithm requires a minimum of two Landsat scenes; one at the beginning and one at the end of the observation period, enabling the development of a change mask for input to the algorithm. The change mask is used to delineate the spatial extent of disturbance events occurring within the time frame represented by the Landsat image pair. The date of disturbance is then determined from a series of MODIS images, usually acquired at eight-day time steps between the dates of the Landsat images. STAARCH also uses a Landsat-derived land cover classification product to identify the expected land cover type of each pixel (from before the disturbance) and assess its reflectance relative to the average reflectance of the given land-cover class. Change detection in STAARCH is restricted to the vegetated land surface, with change features suppressed for non-vegetated land cover classes.

2.2. Detection of spatial changes per land cover type

The spatial delineation of disturbance features is determined by STAARCH at 30 m spatial resolution using a change mask derived from Landsat imagery. Change detection is performed using the Disturbance Index (DI) described in Healey et al. (2005), an index specifically designed to detect changes in forested land cover types. The DI is a transformation of the Tasseled Cap data space and is calculated using the three Tasseled Cap indices (brightness, greenness and wetness) from Landsat TM/ETM+ data (Crist & Kauth, 1986; Healey et al., 2005; Kauth & Thomas, 1976; Masek et al., 2008). At a basic level, the DI records the normalized spectral distance of any given pixel from a nominal “mature forest” class to a “bare soil” class (Healey et al., 2005). The index is computed as a linear combination of the three normalized Tasseled Cap values:

$$B_r = \frac{B - \bar{B}}{B_\sigma} \quad (1)$$

$$G_r = \frac{G - \bar{G}}{G_\sigma} \quad (2)$$

$$W_r = \frac{W - \bar{W}}{W_\sigma} \quad (3)$$

where B_r , G_r , W_r are the normalized (rescaled) brightness, greenness, and wetness, indices respectively, and \bar{B} , \bar{G} and \bar{W} and B_σ , G_σ , W_σ are mean and standard deviation of these three Tasseled Cap spaces. The re-scaling process normalizes pixel values across Tasseled Cap bands with respect to overall changes in reflectance, such as seasonal

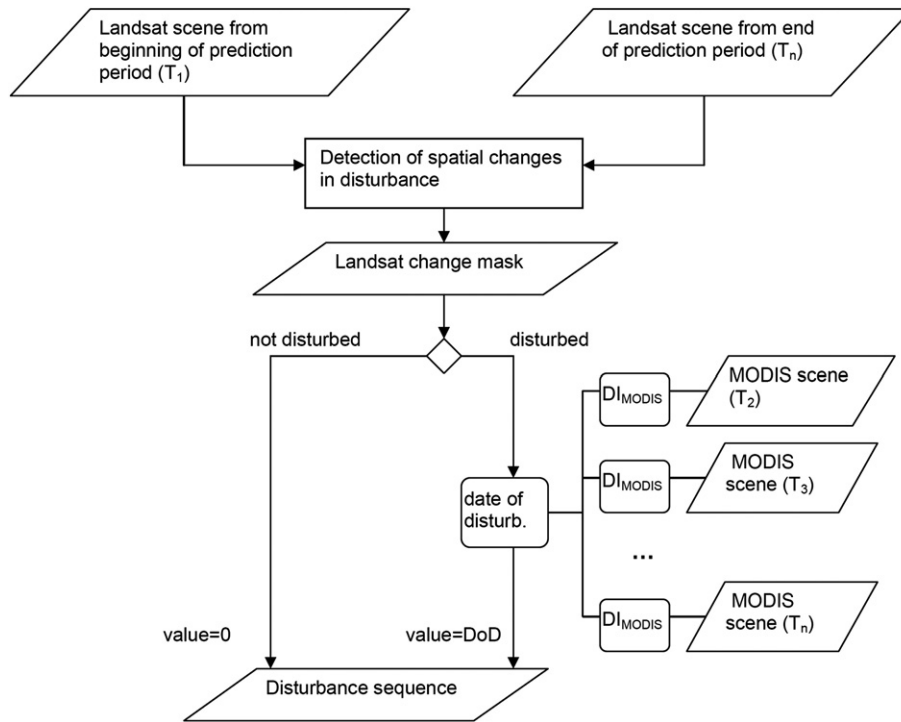


Fig. 1. Flow chart of the STAARCH implementation. The algorithm is based on a two step implementation; the spatial extend of land cover disturbance is determined first using yearly Landsat imagery and disturbed pixels are being flagged.

changes or changes induced by directional reflectance effects, thereby effectively minimizing seasonal variability in the imagery. The Disturbance Index ($DI_{Landsat}$) is then defined as a linear combination of the three normalized Tasseled Cap spaces (Healey et al., 2005):

$$DI_{Landsat} = B_r - (G_r + W_r). \quad (4)$$

In their original algorithm, Healey et al. (2005) computed \bar{B} , \bar{G} and \bar{W} as arithmetic mean of all forested pixels which were identified from pre-existing maps, and defined disturbance by thresholding $DI_{Landsat}$. While this technique has proven useful for forested environments (Healey et al., 2005) it may be less suited to detect disturbances in more heterogeneous landscapes as the natural variability of B_r , G_r , W_r is expected to be relative high. In STAARCH, an external land cover classification product was used to compute the mean and standard deviation of the three Tasseled Cap spaces separately for each vegetated land cover type. This technique was applied to minimize the standard deviation used to normalize B_r , G_r , W_r while increasing the sensitivity of $DI_{Landsat}$ to individual disturbance events.

To verify the vegetation cover of a given pixel, a normalized difference vegetation index ($NDVI_r$) is computed relative to the mean of the NDVI of each land cover type, in a manner analogous to Eqs. (1)–(3):

$$NDVI_r = \frac{NDVI - \overline{NDVI}}{NDVI_{\sigma}} \quad (5)$$

where \overline{NDVI} and $NDVI_{\sigma}$ are the mean and standard deviation the NDVI of each land cover class, respectively. Landsat pixels are flagged as “disturbed” if a series of three conditions were fulfilled:

1. The DI of a pixel reaches a given threshold; in this study, we selected a value of +2, which roughly corresponds to units of standard deviation used for normalizing the forest population (Healey et al., 2005; Masek et al., 2008). Pixels must start below this DI threshold before reaching it in order to be flagged as disturbed.

2. The DI of at least one of its immediate neighbours also reaches this threshold. This condition acts to reduce the amount of noise in the image through elimination of pixel outliers
3. The normalized Tasseled Cap brightness, wetness, and NDVI, do not exceed a specified threshold. This condition is implemented to reduce noise in the transition zones between vegetated and non-vegetated land cover classes and possible noise related to shading effects. In this study we chose values of −3, −1 and 0, for B_r , W_r and $NDVI_r$, respectively (for instance, a logged or burned area is unlikely to show an increase in $NDVI_r$ or a large decrease in brightness or larger increase in wetness).

2.3. Automated detection of cloud contamination in Landsat scenes

Disturbance of vegetation for temporally obscured areas such as due to cloud or snow contamination is challenging (Irish et al., 2006), and as a result an automatic method was used for identifying and excluding these areas. The cloud and snow cover mask implemented in STAARCH is based on the Automated Cloud-Cover Assessment (ACCA) algorithm (Irish, 2000; Irish et al., 2006). ACCA uses a series of eight filtering techniques to identify cloud contamination and snow cover in Landsat data based on reflectance brightness, surface temperature (from the Landsat thermal band) and several band ratios to eliminate highly reflective vegetation, senescing vegetation, and highly reflective rocks and sands. The core of ACCA is a Landsat Band 5/6 (Mid-IR/Thermal-IR) composite to identify cold, yet highly reflective areas (i.e., clouds and snow) (Irish, 2000), with snow being distinguished from clouds by means of the normalized difference snow index (NDSI) (Hall et al., 1995) based on the reflectance of band 2 and 5 (Green and Mid-IR wavelengths).

2.4. Detection of temporal changes in land cover

The implementation of STAARCH is based on the MOD09/MYD09 product, which provides eight-day composites of daily MODIS surface reflectance, thereby effectively minimizing cloud contamination

Table 1
Tasseled Cap coefficients for MODIS (Zhang et al., 2002).

Band name	Red	Near-IR	Blue	Green	M-IR	M-IR	M-IR
MODIS (nm)	620–670	841–876	459–479	545–565	1230–1250	1628–1652	2105–2155
Brightness	0.3956	0.4718	0.3354	0.3834	0.3946	0.3434	0.2964
Greenness	−0.3399	0.5952	−0.2129	−0.2222	0.4617	−0.1037	−0.46
Wetness	0.10839	0.0912	0.5065	0.404	−0.241	−0.4658	−0.5306

present in daily MODIS acquisitions (Vermote et al., 1997; Vermote & Kotchenova, 2008). For reasons of compatibility, it is desirable to extract similar disturbance information from Landsat and MODIS in order to facilitate the identification of particular disturbance events. As opposed to the Landsat Tasseled Cap transformation which is based on Landsat bands 1–5 and 7, Zhang et al. (2002) demonstrate the use of the seven MODIS land bands to extract disturbance information at a 500 m spatial resolution. Table 1 gives an overview of the MODIS-based Tasseled Cap coefficients (Zhang et al., 2002).

The MODIS-derived Tasseled Cap data spaces for brightness, greenness and wetness are used by STAARCH to compute a DI_{MODIS} analogous to the DI obtained from Landsat (Healey et al., 2005). The normalization process (Eqs. (1)–(3)) was, however, simplified to use the arithmetic mean and standard deviation of all vegetated land cover classes, instead of differentiating between individual vegetation types. The reason for this is that MODIS, with its 500 m spatial resolution, will almost always observe a mixture of different land cover types within a given pixel. A certain decline in disturbance predictability can be expected when comparing Landsat and MODIS imagery (Collins & Woodcock, 1996; Jin & Sader, 2005; Zhan et al., 2002; Pape & Franklin, 2008) owing to the differences in spatial resolution and signal-to-noise ratio of both sensors. When aided by the Landsat-derived change mask, however, we hypothesized that, at least to up to a certain degree, the MODIS-based disturbance index should indicate the time interval at which a particular disturbance event occurred, even if the disturbed area is below the size of a MODIS pixel, since there should still be a noticeable increase in DI_{MODIS} .

STAARCH identifies the date of disturbance (DoD) of a flagged pixel (that is, a pixel marked as disturbed using $DI_{Landsat}$) by computing a moving average of the DI values of each of three subsequent MODIS composites collected in between the two Landsat acquisition dates ($\overline{DI_{MODIS}}$). For instance, the first disturbance value in such a MODIS time sequence ($\overline{DI_{MODIS_1}}$) is computed using the first three MODIS scenes acquired following the first Landsat scene, the second DI value ($\overline{DI_{MODIS_2}}$) is computed using MODIS scenes 2–4, and so on. The 8 day time period at which a given pixel was disturbed is then identified by comparing each $\overline{DI_{MODIS}}$ value for this pixel $\overline{DI_{MODIS(1..n)}}$ to the minimum and maximum ($\overline{DI_{MODIS_{MIN}}}$ and $\overline{DI_{MODIS_{MAX}}}$) of all $\overline{DI_{MODIS}}$ values within the sequence:

$$\overline{DI_{MODIS}} \geq \overline{DI_{MODIS_{MIN}}} + t(\overline{DI_{MODIS_{MAX}}} - \overline{DI_{MODIS_{MIN}}}) \quad (6)$$

where t is the threshold value to identify land cover change, for this study it was defined as $t = \frac{2}{3}$. The time of disturbance is determined from the first $\overline{DI_{MODIS}}$ that satisfy the above condition (Eq. (6)). The MOD09/MYD09 quality flags were used to determine cloud contamination and other low-quality pixels, and low-quality values were then automatically eliminated from the disturbance detection.

2.5. Algorithm outputs

The main output of STAARCH is a disturbance sequence image in which all pixels that have been flagged as disturbed are assigned an integer value which corresponds to the 8-day time interval at which a disturbance event occurred. For instance, if a pixel has been most likely disturbed at T_5 in a given MODIS sequence $T_1...T_n$ (with n being

the total number of MODIS images acquired) this pixel will be assigned a value of 5. Pixel values of areas that haven't been disturbed at all are assigned a value of 0 (Fig. 1). Optionally, intermediate results, such as the Landsat change mask and the Landsat and MODIS-derived disturbance indices can also be written to file.

STAARCH also allows the output of synthetic 30 m Landsat-like predictions of surface reflectance, based on the STARFM algorithm (Gao et al., 2006). (Please note, the term “prediction” is used in this paper in the context of estimating high resolution reflectance by fusing multiple data sources). STARFM generates Landsat-like, or synthetic Landsat, images from a spatially weighted difference computed between a Landsat and a MODIS scene acquired at a base date (T_1), and one or more MODIS scenes acquired at a prediction date (T_p). In the implementation of Gao et al. (2006), spectral information from the Landsat-7 ETM+ or Landsat-5 Thematic Mapper sensor was synthesized to match the locations of Landsat ETM+ bands 1–5 and 7 with their corresponding MODIS land bands. A moving window technique was used to minimize the effect of pixel outliers using the spatially weighted mean of all pixels within the window area. Either surface or top-of-atmosphere reflectance may be used, provided the comparable products are used for both the MODIS and Landsat inputs.

In the original STARFM model, changes were considered by introducing a temporal (changing) weight. This weight was defined as the combination of distance weight, spatial weight and temporal weight. Temporal weight was determined by the changes of predicting MODIS data between two input data pairs. The input data pair with less change in MODIS observations would receive the higher weight. This technique has proven useful for detecting gradual changes occurring over larger areas such as seasonal changes in vegetation cover (Gao et al., 2006), but it seems less optimized to detecting disturbances that occur fast and are restricted to smaller areas. This is due to the coarse spatial resolution of MODIS and due to the fact an image acquired after a disturbance event will only obtain higher temporal weights when the time span between the actual disturbance event and the MODIS acquisition data is significantly shorter than that between the disturbance and the acquisition date from the MODIS scene before this event. As a result of these considerations, a significant change to the STARFM algorithm as introduced by Gao et al. (2006) was made in that the base image pair (T_1) upon which a prediction is made is now being composed of the first (T_1) and the last (T_n) MODIS and Landsat scenes of a given time series, depending upon which image pair best describes the land cover situation of a given pixel at the time of prediction. For instance, if the prediction date of an image lies before a particular area was disturbed ($T_p < DoD$), then the base information for a pixel in this area will be derived from the first Landsat and MODIS scene (T_1), because this image pair better represents the land cover type for the prediction date in this area. Conversely, if a pixel value is being predicted for the time after a given

Table 2
Landsat acquisition dates.

Sensor	Acquisition date
Landsat ETM	2002/08/08
Landsat ETM	2004/08/13
Landsat ETM	2005/09/17

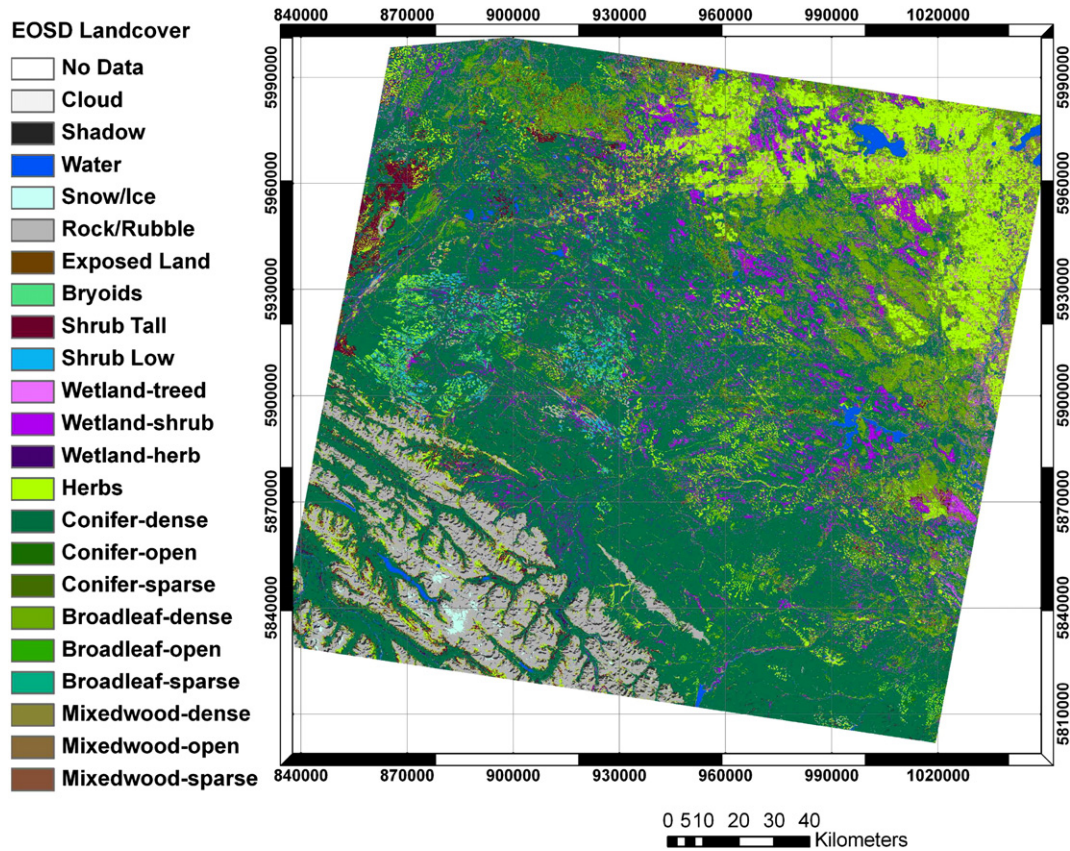


Fig. 2. Map of the EOSD land cover types found in the study area. The most dominant land cover type in the study area is dense coniferous forest (51%), followed by dense broadleaf forest cover and herbs (10% each) and 8% wetland in the north-west. About 10% of the total land cover is classified as non-vegetated surface (rock, snow/ice and water).

area was disturbed ($T_p \geq \text{DoD}$), the base information for the pixels in this area will be derived from the last MODIS and Landsat image pair (T_n) as this pair will consider the detected change in land cover in this

area. Reflectance values for pixels that have not been flagged as disturbed are being predicted from the first Landsat and MODIS scene (Gao et al., 2006).

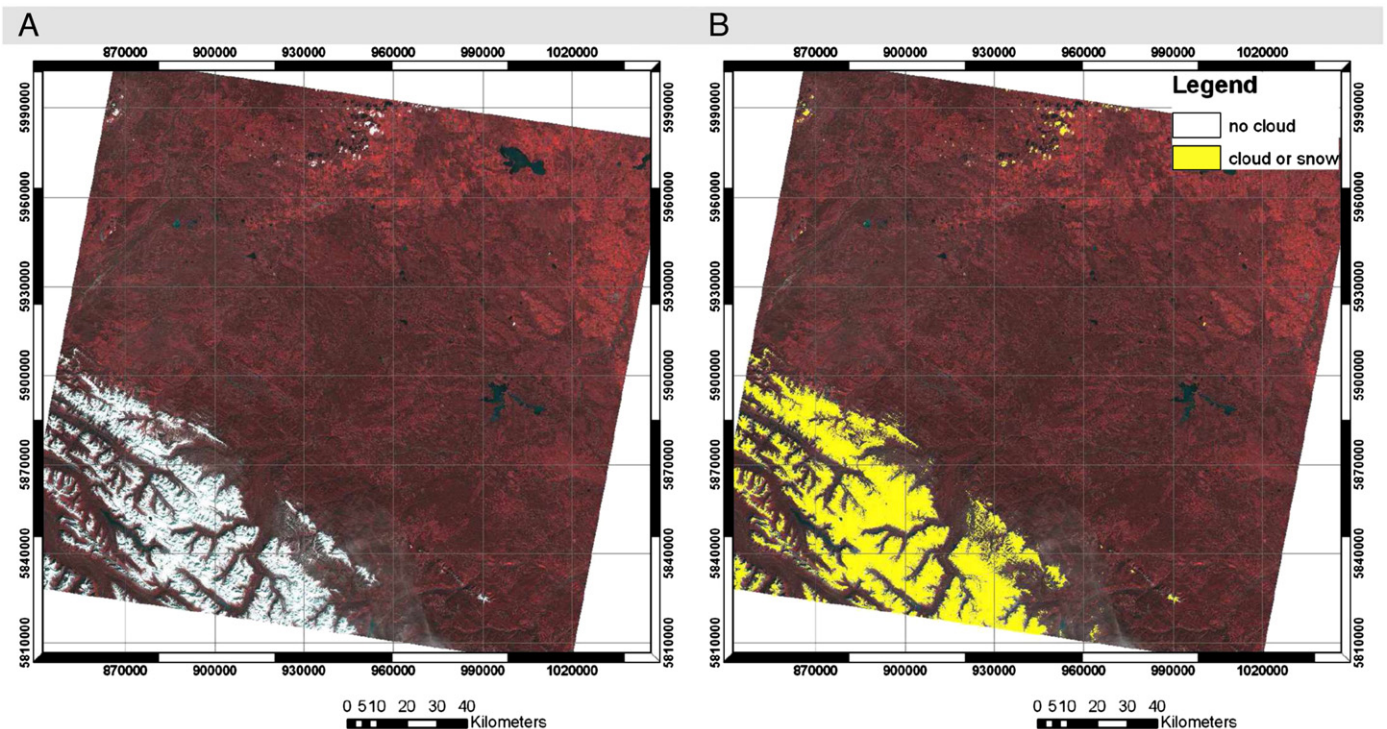


Fig. 3. Cloud and snow mask ACCA for the 2005 Landsat image.

3. Algorithm testing

3.1. Image data

The algorithm was applied at a site in west-central Alberta, Canada ($53^{\circ} 9' N$, $116^{\circ} 30' W$) corresponding to WRS-2 Path 44/Row 23 for which the types and year of disturbance were known and could be validated using an independent data source described below. Three cloud-free (cloud cover <10%) Landsat-5 TM scenes were acquired between 2002 and 2005 (Table 2) through the USGS GLOVIS portal

(<http://glovis.usgs.gov/>). The images were atmospherically corrected using the cosine approximation model (COST) (Chavez, 1996; Wu et al., 2005) and radiometrically normalized (Hall et al., 1991) with respect to the 2005 imagery in order to simplify the comparison between the data.

A total of 110 eight-day MODIS composites (MOD09A1/MYD09A1) with a spatial resolution of 500 m were obtained from the EOS data gateway of NASA's Goddard Space Flight Center (<http://redhook.gsfc.nasa.gov>) for the growing season (March 15th–October 15th) between 2002 and 2005. The MODIS data were reprojected to

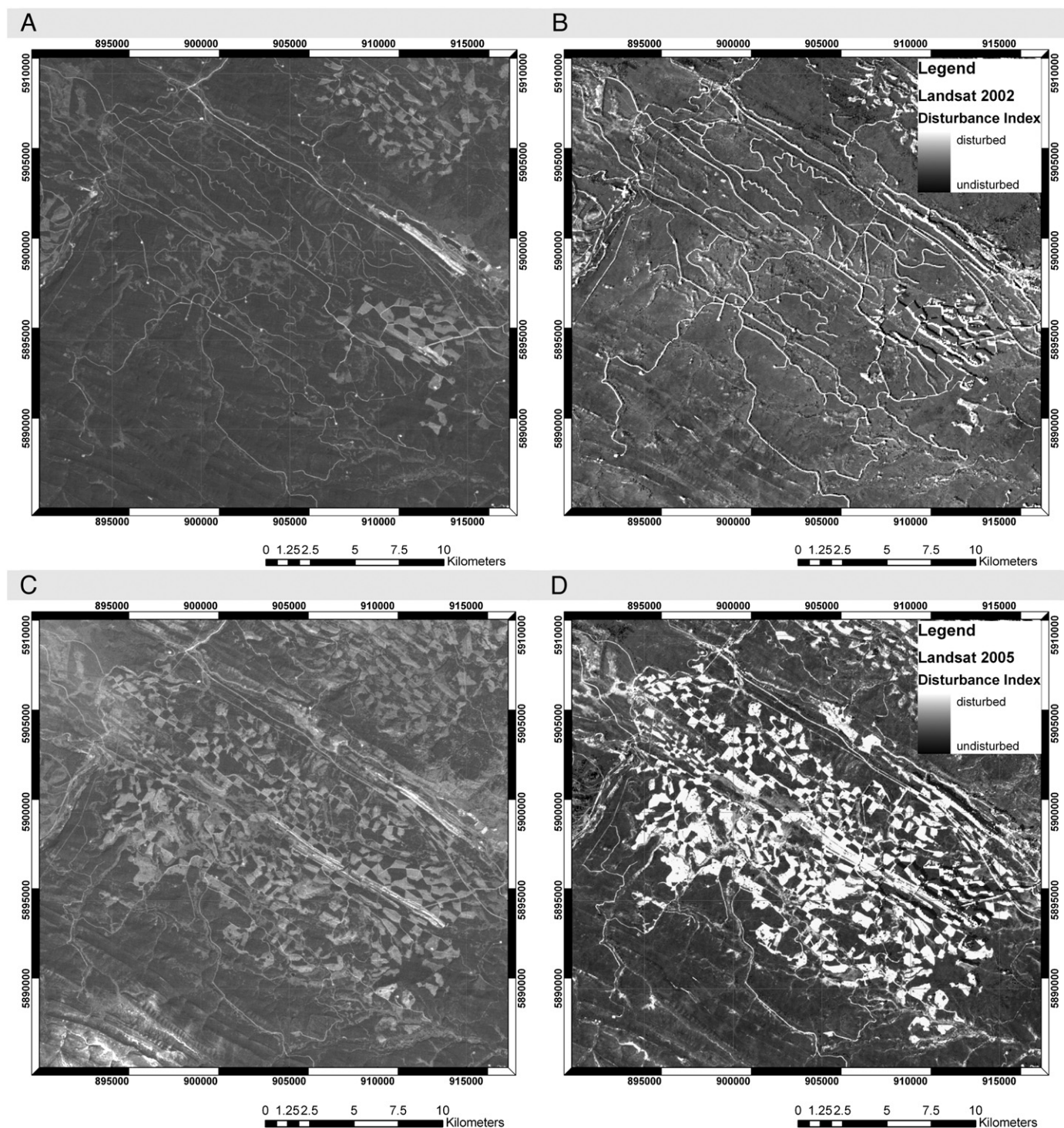


Fig. 4. Comparison between Landsat TM reflectance (Band 3) in 2002 (A) and 2005 (C) and the disturbance index computed for these two observations (B and D, respectively). Dark $DI_{Landsat}$ pixels correspond to undisturbed areas, disturbances are highlighted in white.

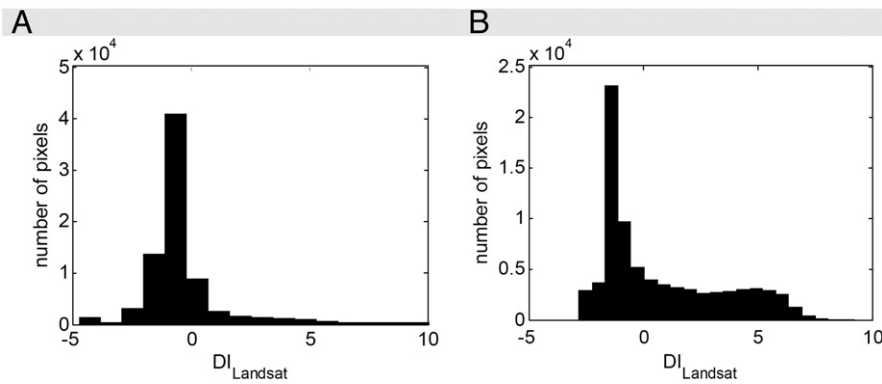


Fig. 5. Pixel distribution of the 2002 (A) and the 2005 (B) $DL_{Landsat}$ image for the example of the focus area shown in Fig. 4. While the largely undisturbed scene in 2002 yields a nearly normal distribution of the pixel values, the 2005 image is skewed towards the positive end of the pixel range.

the Universal Transverse Mercator (UTM) projection using the MODIS reprojection tool (Kalvelage & Willems, 2005), clipped to the extent of the available Landsat imagery, and resampled to a 30 m spatial resolution using a nearest neighbour approach.

3.2. Land cover classification

In this implementation of STAARCH, we used a Landsat-7 land cover classification of the forested area of Canada produced for the Earth Observation for Sustainable Development of Forests (EOSD) initiative, a collaboration between the Canadian Forest Service and the Canadian Space Agency (Wulder et al., 2003), aided by support from all provinces and territories. The EOSD land cover classification product is based upon unsupervised classification, hyperclustering,

and manual labelling of Landsat TM and ETM+ data, thereby facilitating the classification of land cover types over larger areas (Franklin and Wulder, 2002; Slaymaker et al., 1996; Wulder et al., 2003). The EOSD product represents circa year 2000 conditions, and captures land cover information based on 30 m spatial resolution Landsat imagery, with products resampled to 25 m. EOSD land cover data were downloaded from the EOSD data portal (http://www4.safar.org/eosdlcp/nts_prov.html) and clipped to the extent of the study area. The particular EOSD product utilized for this study is based upon a Landsat image collected in 2002. Fig. 2 contains an overview of the dominant land cover types present in the image, mainly coniferous forest (comprised of largely of lodgepole pine (*Pinus contorta* var. *latifolia*), and white spruce (*Picea glauca*) with some presence of Douglas-fir (*Pseudotsuga menziesii* var. *menziesii*) with

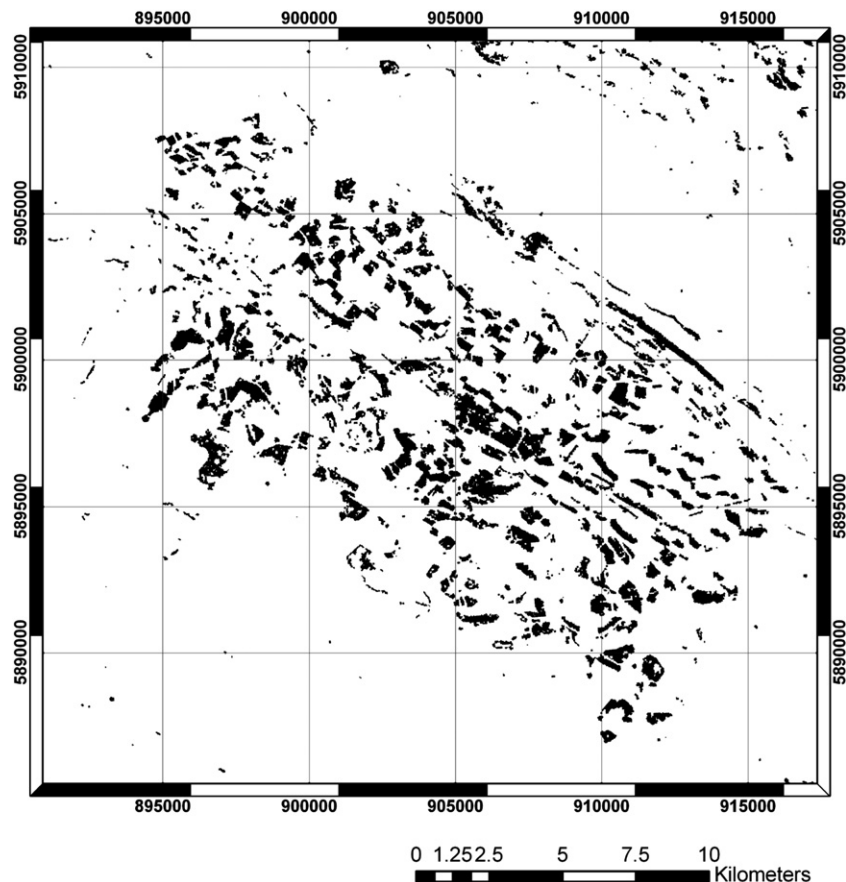


Fig. 6. Landsat derived change mask between 2002/08/08 and 2005/09/21. The mask was derived from the difference in disturbance of the two Landsat images. The area shown in this example corresponds to the image shown in Fig. 4.

subsidiary herbal and shrub vegetation and patches of water and rocks. Land cover patches are generally large, the landscape can, however, be quite heterogeneous within some areas due to harvesting activities and related cut blocks and access road networks.

3.3. Disturbance validation data set

We acquired the validation data set from a disturbance inventory feature database developed by the multi-annual disturbance mapping project of Linke et al. (in press). This project delineated forest-replacing

disturbance features in polygon-vector format from annual difference layers, derived from an annual series of summer Landsat Thematic Mapper and Enhanced Thematic Mapper Plus spanning the years 1998 to 2005. The inventory contains information on the year of origin and type of individual disturbance events, obtained using an integrated approach of automated segmentation and manual digitization methods described fully in Linke et al. (in press). Areal disturbance features (cut blocks, mines, forest fires) were identified through automatic segmentation of thresholded difference images, which provided the basis for delineating individual disturbance entities. These features were

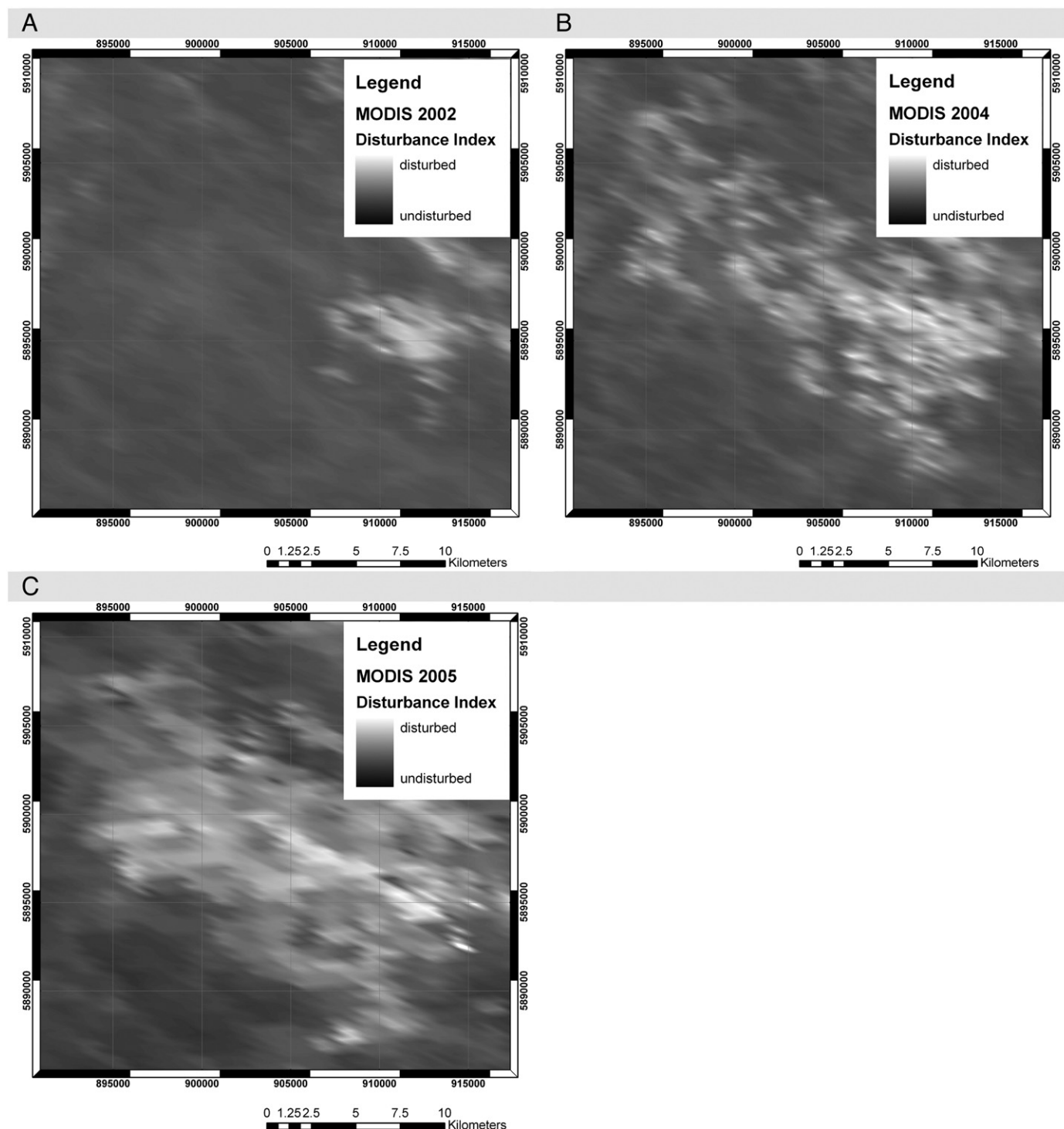


Fig. 7. MODIS-derived disturbance index (DI_{MODIS}) for the example of the MODIS scenes acquired at 2002/08/13, 2004/08/13 and 2005/09/22, respectively. Bright pixel values correspond to the disturbances, the pattern shown in Fig. 4 is clearly observable also from these coarser spatial resolution images.

subsequently labeled on the basis of size, shape and context. Delineations and classifications were visually compared with the Landsat imagery and manually cleaned where necessary. Because of the high precision applied during manual verification, and specialized boundary-alignment corrections (see Linke et al., 2009), the detection accuracy of this validation data set was assessed at 100%, and the classification accuracy was 98% (Linke et al., *in press*).

3.4. Validation experiment

STAARCH is designed to predict changes in land cover and disturbance at eight-day time steps, based upon the availability of MOD09/MYD09 composites. We designed a validation protocol of STAARCH using the disturbance validation data set (Section 3.3) in order to test the capability of STAARCH to correctly determine DoD across a multi-year time period using MODIS. The validation protocol was applied under the assumption that if stand-replacing disturbance information could be correctly extracted from eight-day MODIS data at yearly time steps, it follows that they could also be derived at higher temporal resolutions with transferable accuracy results, since the underlying physics (sensor properties) and the prediction algorithm remain unchanged. Note that this assumption is reasonable only for stand-replacing disturbance events for which the spectral changes due to disturbance are expected to be much greater than seasonal changes in vegetation cover. The effect of seasonal variation is minimized through the land cover normalization process described above.

In this study we used Landsat scenes from 2002 and 2005 to capture the disturbances that occurred during these years in the study area and the intervening MODIS scenes to predict their DoD. The predictions were then compared to the year of disturbance known

from the validation disturbance dataset and the percentage of the correctly classified disturbed area was determined. The Landsat scene acquired at 2004/08/13 was not used for predicting disturbances and was set aside for validating the disturbance predictions made in STAARCH. An area of 1500 m × 1500 m was selected as the moving window size for synthetic Landsat predictions and the uncertainties of Landsat and MODIS surface reflectance were set to 0.002 and 0.005 for the visible and the NIR bands, respectively (Gao et al., 2006).

4. Results

4.1. Mapping the spatial extent of disturbances

The cloud cover algorithm used in STAARCH successfully detected cloud and snow cover in the selected Landsat scenes, thereby masking and excluding areas of high uncertainty that are frequently the site of false positive error. Fig. 3 shows the result of the cloud and snow cover assessment implemented in STAARCH for the example of the 2005 Landsat image. The original Landsat scene is shown in Fig. 3A, with the inset in 3B enabling a comparison to the superimposed cloud and snow-cover mask. The ACCA algorithm implemented in STAARCH accurately identified cloud and snow cover in the image, with the exception of a small hazy area (covering about 0.5% of the image) in the southern part of the scene.

DI_{Landsat} effectively highlighted disturbance information at a 30 m spatial resolution. Fig. 4A shows the reflectance of the green Landsat channel as observed in 2002, with a few cut blocks and access roads visible in the image (for illustration purposes, only a small subset of the entire scene is shown). Fig. 4B shows the disturbance index computed from the 2002 Landsat scene, wherein the bright areas correspond to the

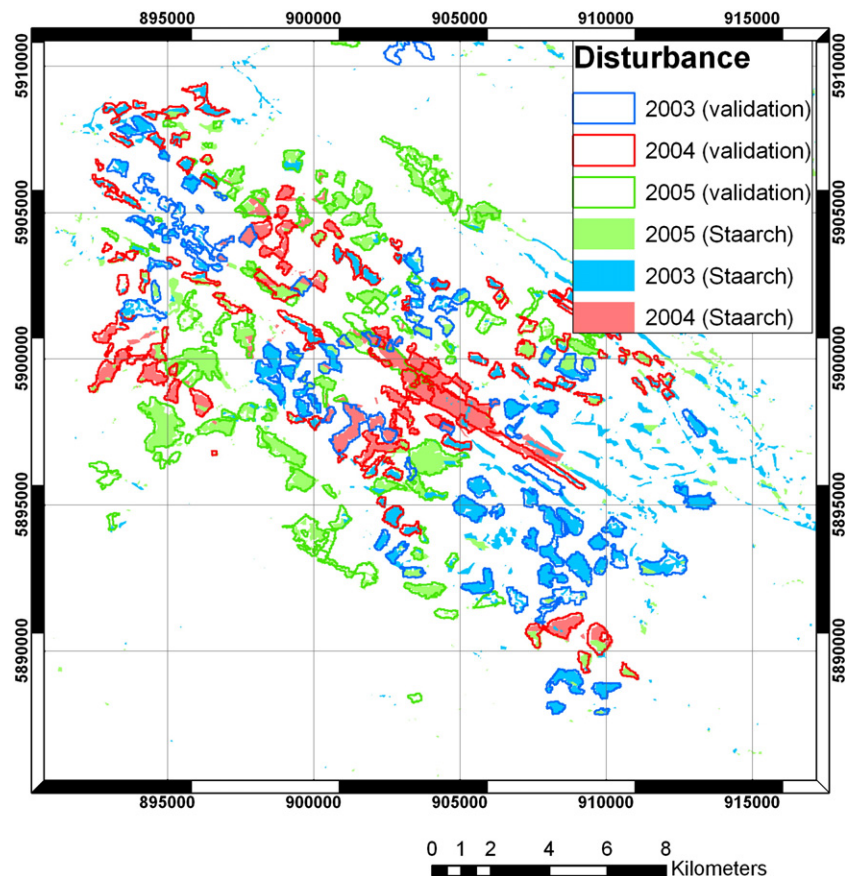
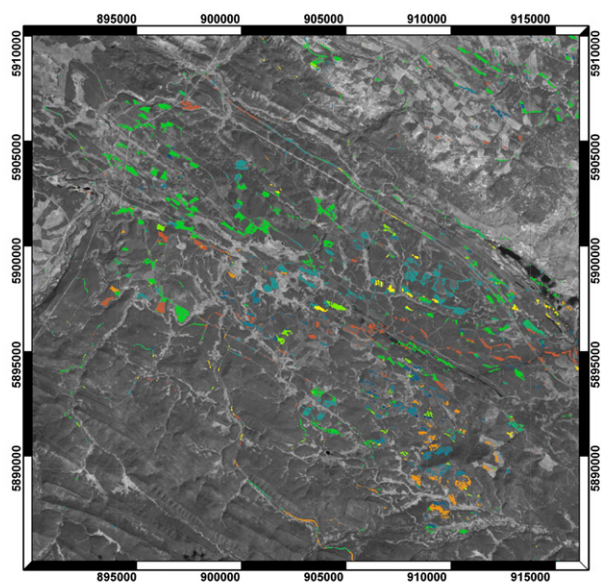
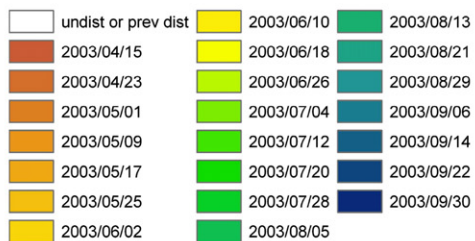
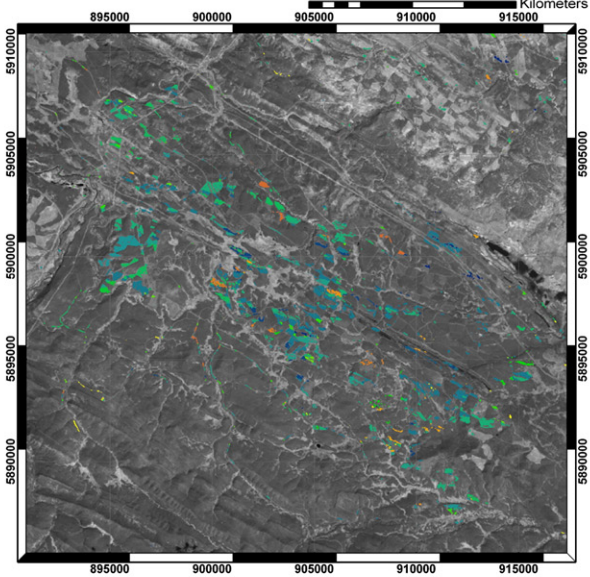
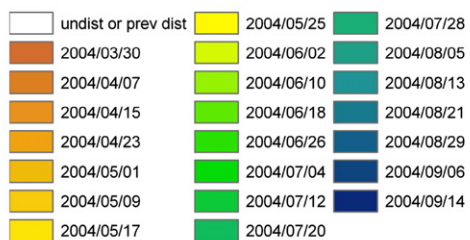


Fig. 8. Comparison between yearly disturbances derived from the validation data set and STAARCH determined year of disturbance. The date of disturbance for all polygons, that show the same color for outline and fill, has been correctly identified by the algorithm; polygons that show a different outline color than filling have been misclassified by STAARCH. The area of correctly identified disturbances was 87%, 87% and 89% in 2002, 2003 and 2005, respectively.

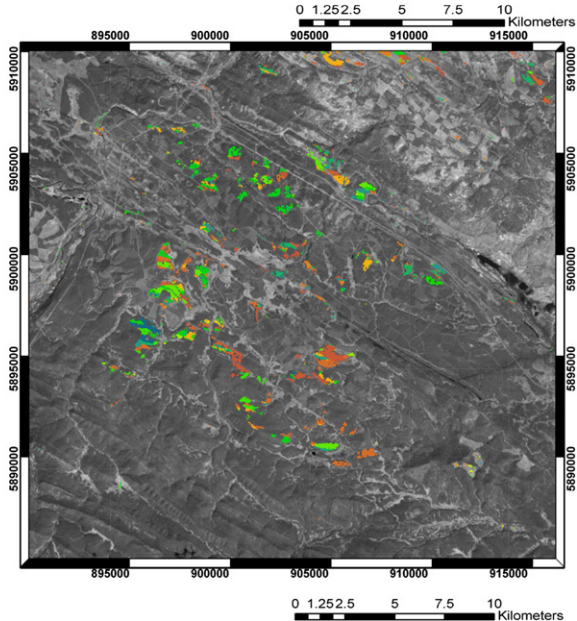
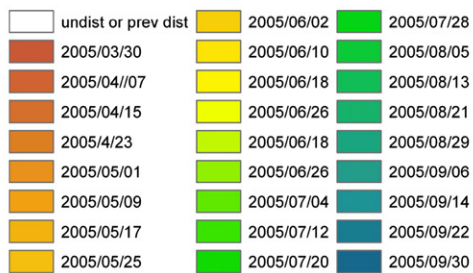
A

Disturbances 2003

B

Disturbances 2004

C

Disturbances 2005

disturbance visible in Fig. 4A. The number of cut blocks increased notably between 2002 and 2005 (Fig. 4C). Fig. 4D illustrates the DI of the 2005 Landsat image, revealing that the index effectively highlighted the disturbances shown in Fig. 4C. Disturbance events caused considerable shifts in the range of $DI_{Landsat}$ on a local scale, illustrated by the histograms of the pixel distribution of $DI_{Landsat}$ for the area shown in Fig. 4 (Fig. 5A and B). While the relatively undisturbed scene in Fig. 4B yields a near normal distribution of $DI_{Landsat}$ values, the distribution of $DI_{Landsat}$ found in Fig. 4D is skewed towards the positive end of the pixel range. However, the average Tasseled Cap values used to normalize $DI_{Landsat}$ per land cover class over the entire scene remained almost constant between 2002 and 2005.

Fig. 6 gives an example of the change mask derived from $DI_{Landsat}$ showing all areas that were disturbed between 2002/08/08 and 2005/09/22. The area shown in the figure corresponds to the area shown in Fig. 4. Over the entire scene, the Landsat-based disturbance algorithm successfully identified 93% of the total disturbed area delineated by the validation data set. The average size of disturbance features detected was 104,790 m², or 0.41 MODIS pixels, with a standard deviation of 195,764 m², or 0.78 MODIS pixels.

4.2. Mapping the date of disturbance

The MODIS disturbance index (DI_{MODIS}) was successfully used to highlight disturbance events in the eight-day composites. Fig. 7A–C shows an example of DI_{MODIS} computed for three MODIS scenes acquired at 2002/08/13, 2004/08/13 and 2005/09/22, respectively. In the Fig. 7 series, the bright areas correspond to the disturbances shown in Fig. 4. The gradual increase in the total area disturbed can be observed also in these coarse-spatial-resolution images. The DI_{MODIS} values were a slightly higher compared to those derived from the Landsat images ($\overline{DI_{MODIS}} = 0.30$, $\sigma = 0.15$ for the MODIS scene acquired at 2002/08/13; $\overline{DI_{MODIS}} = 0.26$, $\sigma = 0.13$; for the MODIS scene acquired at 2004/08/13, and $\overline{DI_{MODIS}} = 0.31$, $\sigma = 0.13$ for the MODIS scene acquired at 2005/09/22).

STAARCH was able to predict the date of disturbance in the 185 km × 185 km test area with a high level of accuracy. Fig. 8 shows a comparison between the disturbance sequence acquired from STAARCH (predicted at a yearly resolution) and the dates acquired from the validation disturbance dataset. The color of the polygon outline corresponds to the year of disturbance determined from the validation data set; the color of the polygon hatch corresponds to the year of disturbance acquired from STAARCH. A spatial intersection of validation dataset- and STAARCH-derived disturbance polygons showed that the model was able to correctly identify 88%, 87% and 89% of the newly disturbed area at the correct time in 2003, 2004 and 2005, respectively. The mean area of correctly classified disturbances over the three years was 169,265 m² or 0.69 MODIS pixels $\sigma = 262,439$ m² (=1.04 MODIS pixels). The mean area of those disturbances that remained unidentified was 47,408 m² or 0.19 MODIS pixels $\sigma = 43,275$ m² (=0.17 MODIS pixels). The total area of misclassified disturbances throughout the entire Landsat scene was <10,750 m² or <0.04% of the total study area.

Fig. 9A–C shows three eight-day sequences of the disturbance events in 2003, 2004 and 2005, respectively. The colors of the disturbed areas correspond to the eight-day time intervals at which disturbances were predicted to have occurred. Fig. 10 shows an overview of the total disturbed area per eight-day time step for 2003, 2004 and 2005, respectively. Disturbance events typically occurred during the early summer months, while the total disturbed area per eight-day interval, as depicted in Fig. 10, decreases towards the end of the growing season. The peak in disturbance activity found in the mid-

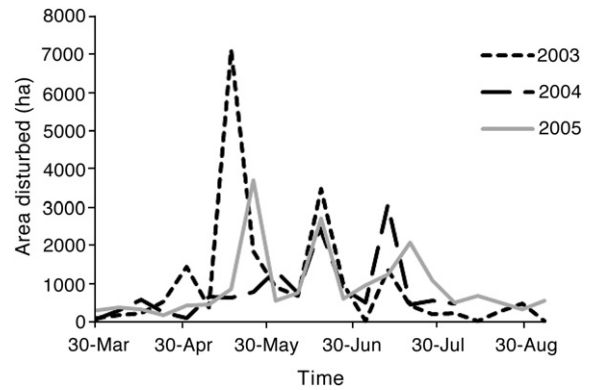


Fig. 10. Total disturbed area per 8 day time step for 2003, 2004 and 2005, respectively. Most disturbance events occurred during the early summer months, while the total disturbed area per 14 day interval decreases towards the end of the growing season. The peak in the mid-May data from 2003 corresponds to a wildfire occurring in the south western region of the Landsat image.

May, 2003, corresponds to a wildfire that occurred in the south western region of the Landsat image.

4.3. Comparison to STARFM

The change detection algorithm implemented in STAARCH is considerably different to the prediction of surface reflectance based on STARFM. Fig. 11A shows the observed Landsat scene acquired at 2004/08/13. Fig. 11B shows the corresponding STARFM prediction using an unmodified version of the algorithm as described by Gao et al. (2006). While the prediction yields a high quality 30 m image, the algorithm fails to describe the temporal aspect of disturbance (at least at a sub-pixel range), since only those regions that were already disturbed in the 2002 Landsat base scene were predicted with their correct land cover type. All the cut blocks occurring after 2002/08/08 were still modelled as forested. This is not unexpected, since this functionality is beyond the initial STARFM algorithm specification. Fig. 11C shows the prediction result of the modified STARFM algorithm based on STAARCH. The modified algorithm yields a considerably improved description of the disturbances with nearly all disturbance events shown in the original observation (Fig. 11A) also being predicted by the STAARCH algorithm (Fig. 11C).

5. Discussion

This study described the implementation and testing of a new data fusion model used to detect changes in land cover at eight-day time steps and at a 30 m spatial resolution. The algorithm was tested over a 185 × 185 km study area in west-central Alberta, Canada. The Landsat derived cloud cover assessment (Irish, 2000; Irish et al., 2006) was successfully used to mask cloud cover in Landsat images, thereby helping to ensure the quality of STAARCH-derived disturbance predictions. Automated masking of cloud and snow cover is an important prerequisite for the prediction of disturbance events, as changes in land cover can only be assessed for cloud-free observations (Cahalan et al., 2001; Hall et al., 1995). While this study did not specifically investigate the effect of cloud shadow on surface reflectance, no evidence was found that cloud shading would have a noticeable impact on prediction of disturbance events. Further research may be required when more cloud contaminated scenes are being used.

The disturbance index of Healey et al. (2005) proved to be a useful technique for determining the spatial extent of changes in land cover. The accuracy with which spatial changes have been predicted

Fig. 9. Sequences of eight-day disturbance intervals for the year of 2003 (A), 2004 (B) and 2005 (C), respectively. The colors of the disturbed areas corresponds to the 8-day time intervals at which disturbances most likely occurred (derived from STAARCH).

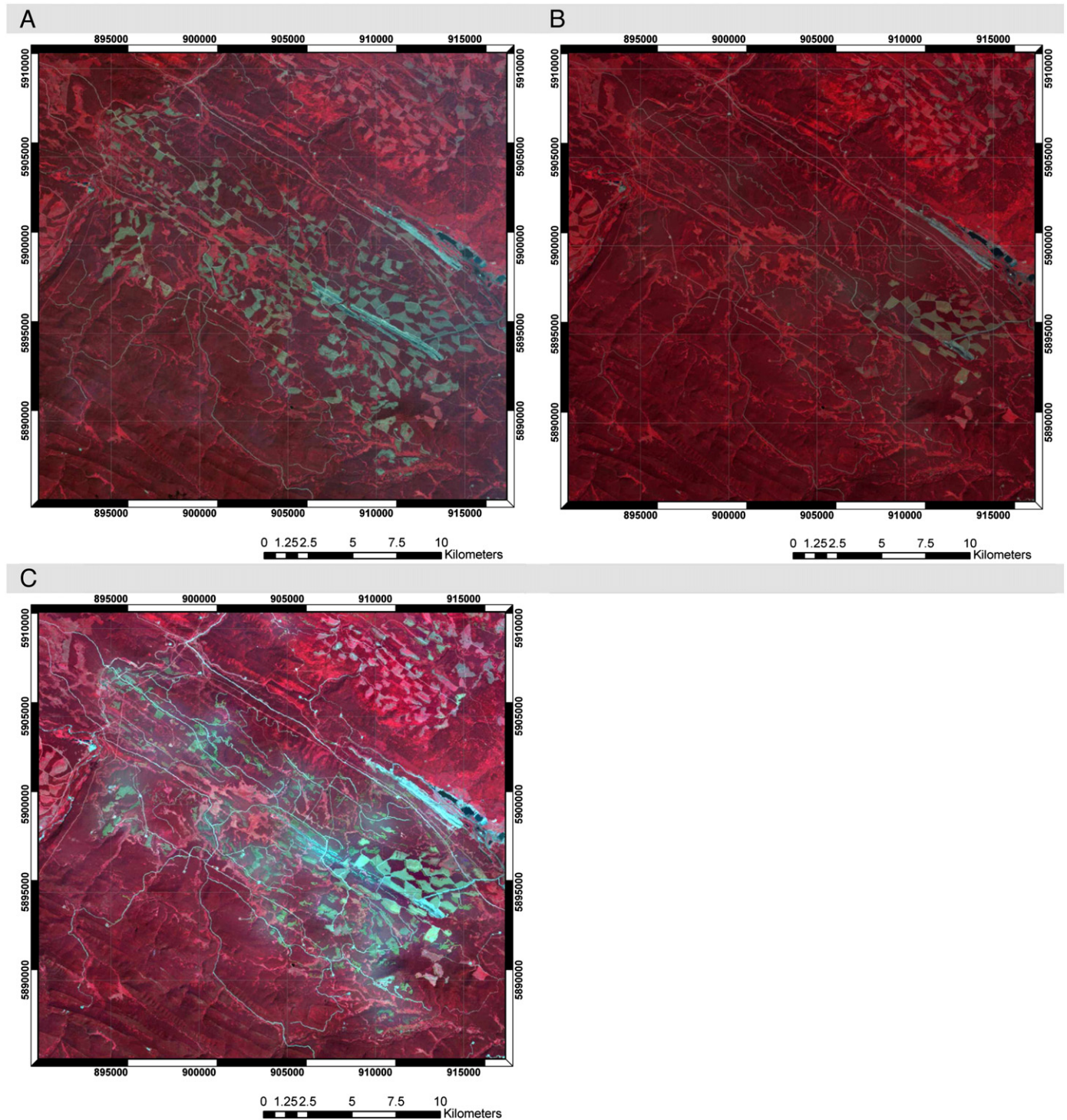


Fig. 11. Landsat scene observed at 2004/08/13. (B) shows the corresponding STARFM prediction using an unmodified version algorithm as introduced by Gao et al. (2006). While the prediction yields a high quality 30 m image, the algorithm fails to describe the newly occurring disturbance events (at least at a sub-pixel range) whereas the STAARCH-derived image (C) includes most of the changes due to Landscape disturbance.

throughout the study area also confirms findings of previous authors (Healey et al., 2005; Masek et al., 2008) and shows that Landsat-based Tasseled Cap transformation is an effective tool for mapping changes in land cover and disturbance. It should be noted, however, that the disturbance index may be less useful in ecosystems types other than forests. For example, disturbances in wetter areas that reveal or result in standing water will likely be not well described by the DI as currently conceived. The results shown in Fig. 6 confirm that $DI = +2$ was an effective threshold for masking disturbance events from the

normalized $DI_{Landsat}$ (Healey et al., 2005). Although this algorithm has proven successful for automated masking of stand-replacing disturbances such as cut blocks or stand-replacing fires, smaller disturbances, such as insect infestations or low-grade fire events, were not examined. Automatic detection of these kinds of disturbances would be useful, particularly in the context of carbon modeling (Kurz et al., 2008). However, these may require further modifications to the detection algorithm (Coops et al., 2006; Franklin et al., 2003; White et al., 2007; Wulder & Dymond, 2003). Other limitations of the

algorithm in its current form include the detection of disturbances smaller than 2 Landsat pixels, as the noise reduction algorithm implemented in the software will limit the size of disturbance features that can effectively be mapped to this resolution. Additionally, detected disturbance events may occur in a more pixelated manner when compared to actual Landsat imagery which shows rather sharp delineation of disturbed areas (for instance in Fig. 4). This is due to the raster based detection algorithm which utilizes coarser spatial resolution imagery.

The MODIS-based Tasseled Cap transformation (Zhang et al., 2003; Zhang et al., 2002) was successfully used in this study to determine the time at which individual disturbance events occurred. Application of the MODIS-derived Tasseled Cap variables (brightness, greenness and wetness) was useful for generating a MODIS-based disturbance index similar to Healey et al. (2005), with a detection accuracy of >87%. The findings shown in Fig. 8 confirm that the applied technique successfully identified disturbances at yearly time steps, however, no validation data was available that would allow the evaluation of DoD at higher temporal resolutions. Additionally, it is apparent from Fig. 8 that there are “false positives” in the image, that is, areas which are shown disturbed in the prediction dataset but not in the validation data. While some these areas have been flagged due to changes in phenology, other disturbances are actually existent but have not been listed in the validation data set such as apparent for some regions in the lower right of Fig. 8. As a result, the proportion of “false positives” is harder to quantify in this dataset.

Evaluation of disturbance events at 8-day time steps would be desirable, but is difficult to realize given the lack of high temporal resolution evaluation data over larger areas. As a result of this limitation to the analysis, Figs. 9 and 10 may be regarded more as a demonstration of what the disturbances might look like when applying MODIS at shorter time intervals. However, since the underlying detection principles are independent of the time steps applied, the results shown in Fig. 9 should in theory be equally applicable to data acquired at eight-day intervals, when only considering stand-replacing disturbance events and over a limited observation period for which vegetation reflectance changes are expected to be smaller than changes due to disturbance events.

The STAARCH algorithm in its present form does not allow for the detection or progression of individual disturbance events. For instance, a cut block may have been established over a few weeks, with its size increasing over time. However, the STAARCH algorithm is limited to a *before and after* delineation of each disturbance event as obtained from Landsat, with the date of disturbance assigned at a much coarser spatial resolution. The date of disturbance determined by the algorithm is therefore more an indicator of when the main disturbance most likely occurred within a MODIS pixel-scale patch, and contains only limited information regarding the time frame over which a disturbance event progressed.

The results of this study have shown that the MODIS disturbance index (DI_{MODIS}) was able to determine the date of disturbance of areas well below the size of a MODIS pixel, which emphasises the capability of this index to capture change events. The detection accuracy of disturbance events from Landsat (93%) and MODIS (87%) are within the range of previous findings (Jin & Sader, 2005; Moody & Woodcock, 1994; Morton et al., 2005; Zhan et al., 2002) and underline the potential of combining these two data sets for prediction of high spatial and temporal resolution disturbance events. It should, however, be noted that those 87% are the results of the yearly validation dataset which was derived from Landsat ETM (Linke et al., *in press*) and the accuracy may be different when observed at 8-day time steps. Because the spatial location of disturbances is predicted exclusively from Landsat, predictions can best be made for the period between two (ideally cloud-free) Landsat observations. This may limit the applicability of the algorithm to timely critical applications. It should also be noted that STAARCH predictions can only be made for those areas which are not obscured by

clouds in either of the used Landsat scenes. This may restrict the applicability of the algorithm where no cloud-free observation exists for a given study period.

The increased level of detail with which STAARCH has produced synthetic Landsat images (Fig. 11) is an important result of this study. It should be noted, however, that the image quality of the predicted scene appears more “hazy” than the observed Landsat data (Fig. 11C vs. Fig. 11A), which is likely due to the mixing of high and low spatial resolution data. This may result in problems for some applications that may rely on more precise estimates of multi-spectral reflectance. Recent results on the fusion of Landsat and MODIS data for the generation of synthetic images suggest that data fusion is a useful technique for predicting seasonal changes in vegetation at a high spatial resolution, and offers new opportunities for infill of cloud or data-gaps resulting from the SLC-off condition of the ETM+ sensor (Gao et al., 2006; Hansen et al., 2008; Hilker et al., *submitted for publication*; Roy et al., 2008). Conventional fusion models are generally not designed to consider stand-level disturbance events. The algorithm introduced in this paper builds upon the proven utility of STARFM to predict high-spatial-resolution synthetic reflectance, while the MODIS-derived change sequence allows the algorithm choose a Landsat/MODIS base date (T_1) that best describes the land cover type of a given pixel at the time of prediction. The resulting improved prediction of surface reflectance can add valuable information for a wide range of applications. Additional algorithm improvements include the capacity to add functionality to identify the type of disturbance. While this research has mainly been focused on forested areas, further research will be required to test the applicability of the presented algorithm in non-forested environments. We expect techniques such as the one introduced in this study will further advance data-blending techniques and the generation of high spatial- and temporal-resolution synthetic spectral observations.

Mapping disturbances with high spatial and temporal resolution has significant potentials for the modeling and ecological applications. For instance, a numerous remote sensing-driven and tower-calibrated ecological models rely upon temporally precise estimates of productivity (GPP, NPP) or gas exchange and, as a result, require accurate reporting of landscape level disturbance on a regular basis (Masek et al., 2008). This advance may offer the community an opportunity to explore the relationship between disturbance and ecosystem processing at more meaningful temporal scales. Other applications include the mapping of wildlife habitats as well as monitoring changes in vegetation biophysical and structural attributes over large areas.

Acknowledgements

Funding for this research was generously provided by the Grizzly Bear Program of the Foothills Research Institute located in Hinton, Alberta, Canada, with additional information available at: <http://www.fmf.ab.ca/>. Much of the Landsat data used in this study was contributed by the U.S. Geological Survey Landsat Data Continuity Mission Project through participation of Wulder on the Landsat Science Team. STARFM algorithm development was supported by NASA Terrestrial Ecology Program and the Landsat Data Continuity Mission Project.

References

- Cahalan, R. F., Oreopoulos, L., Wen, G., Marshak, A., Tsay, S. C., & DeFelice, T. (2001). Cloud characterization and clear-sky correction from Landsat-7. *Remote Sensing of Environment*, 78, 83–98.
- Chavez, P. S. (1996). Image-based atmospheric corrections revisited and improved. *Photogrammetric Engineering and Remote Sensing*, 62, 1025–1036.
- Cohen, W., & Goward, S. (2004). Landsat's role in ecological applications of remote sensing. *BioScience*, 54, 535–545.
- Cohen, W., Spies, T., Alig, R., Oetter, D., Maierseperger, T., & Fiorella, M. (2002). Characterizing 23 years (1972–95) of stand replacement disturbance in western Oregon forests with Landsat imagery. *Ecosystems*, 5, 122–137.

- Collins, J. B., & Woodcock, C. E. (1996). An assessment of several linear change detection techniques for mapping forest mortality using multi-temporal Landsat TM data. *Remote Sensing of Environment*, 56, 66–77.
- Coops, N. C., Johnson, M., Wulder, M. A., & White, J. C. (2006). Assessment of QuickBird high spatial resolution imagery to detect red attack damage due to mountain pine beetle infestation. *Remote Sensing of Environment*, 103, 67–80.
- Crist, E. P., & Cicone, R. C. (1984). A physically-based transformation of thematic mapper data — The Tm Tasseled Cap. *IEEE Transactions on Geoscience and Remote Sensing*, 22, 256–263.
- Crist, E., & Kauth, R. (1986). The Tasseled Cap de-mystified. *Photogrammetric Engineering & Remote Sensing*, 52, 81–86.
- DeFries, R. S., Field, C. B., Fung, I., Collatz, G. J., & Bounoua, L. (1999). Combining satellite data and biogeochemical models to estimate global effects of human-induced land cover change on carbon emissions and primary productivity. *Global Biogeochemical Cycles*, 13, 803–815.
- Foster, D., Swanson, F., Aber, J., Burke, I., Brokaw, N., Tilman, D., et al. (2003). The importance of land-use legacies to ecology and conservation. *Bioscience*, 53, 77–88.
- Franklin, S. E., Lavigne, M. B., Moskal, L. M., Wulder, M. A., & McCaffrey, T. M. (2001). Interpretation of forest harvest conditions in New Brunswick using Landsat TM enhanced wetness difference imagery (EWDI). *Canadian Journal of Remote Sensing*, 27, 118–128.
- Franklin, S. E., & Wulder, M. A. (2002). Remote sensing methods in medium spatial resolution satellite data land cover classification of large areas. *Progress in Physical Geography*, 26, 173–205.
- Franklin, S., Wulder, M., Skakun, R., & Carroll, A. (2003). Mountain Pine Beetle red-attack damage classification using stratified Landsat TM data in British Columbia, British Columbia, Canada. *Photogrammetric Engineering & Remote Sensing*, 69, 283–288.
- Gao, F., Masek, J., Schwaller, M., & Hall, F. (2006). On the blending of the Landsat TM and MODIS surface reflectance: Predicting daily Landsat surface reflectance. *IEEE Transactions on Geoscience and Remote Sensing*, 44, 2207–2218.
- Hall, D. K., Riggs, G. A., & Salomonson, V. V. (1995). Development of methods for mapping global snow cover using moderate resolution imaging spectroradiometer data. *Remote Sensing of Environment*, 54, 127–140.
- Hall, F. G., Strebel, D. E., Nickeson, J. E., & Goetz, S. J. (1991). Radiometric rectification — Toward a common radiometric response among multitemporal, multisensor images. *Remote Sensing of Environment*, 35, 11–27.
- Hansen, A. J., Neilson, R. R., Dale, V. H., Flather, C. H., Iverson, L. R., Currie, D. J., et al. (2001). Global change in forests: Responses of species, communities, and biomes. *Bioscience*, 51, 765–779.
- Hansen, M. C., Roy, D. P., Lindquist, E., Aducci, B., Justice, C. O., & Altstatt, A. (2008). A method for integrating MODIS and Landsat data for systematic monitoring of forest cover and change in the Congo Basin. *Remote Sensing of Environment*, 112, 2495–2513.
- Healey, S. P., Cohen, W. B., Yang, Z. Q., & Krankina, O. N. (2005). Comparison of Tasseled Cap-based Landsat data structures for use in forest disturbance detection. *Remote Sensing of Environment*, 97, 301–310.
- Hilker, T., Wulder, M. A., Coops, N. C., Seitz, N., White, J. C., Gao, F., et al. (submitted for publication). Generation of dense time series synthetic Landsat data through data blending with MODIS using the spatial and temporal adaptive reflectance fusion model (STARFM). *Remote Sensing of Environment*.
- Irish, J. (2000). Landsat 7 automatic cloud cover assessment. In S. S. Shen & M. R. Descour (Eds.), *SPIE/AeroSense 2000, algorithms for multispectral, hyperspectral, and ultrahyperspectral imagery* (pp. 348–355).
- Irish, R. R., Barker, J. L., Goward, S. N., & Arvidson, T. (2006). Characterization of the Landsat-7 ETM+ automated cloud-cover assessment (ACCA) algorithm. *Photogrammetric Engineering and Remote Sensing*, 72, 1179–1188.
- Ju, J. C., & Roy, D. P. (2008). The availability of cloud-free Landsat ETM plus data over the conterminous United States and globally. *Remote Sensing of Environment*, 112, 1196–1211.
- Jin, S. M., & Sader, S. A. (2005). MODIS time-series imagery for forest disturbance detection and quantification of patch size effects. *Remote Sensing of Environment*, 99, 462–470.
- Kalvelage, T., & Willems, J. (2005). Supporting users through integrated retrieval, processing, and distribution systems at the Land Processes Distributed Active Archive Center. *Acta Astronautica*, 56, 681–687.
- Kauth, R., & Thomas, G. (1976). The tasseled cap—A graphical description of the spectral-temporal development of agricultural crops as seen by Landsat. *Proceedings of the Symposium on Machine Processing of Remotely Sensed Data* (pp. 4B–41–4B–51). Indiana: Purdue University of West Lafayette.
- Kurz, W. A., Dymond, C. C., Stinson, G., Rampley, G. J., Neilson, E. T., Carroll, A. L., et al. (2008). Mountain pine beetle and forest carbon feedback to climate change. *Nature*, 452, 987–990.
- Lada, H., Thomson, J. R., Mac Nally, R., & Taylor, A. C. (2008). Impacts of massive landscape change on a carnivorous marsupial in south-eastern Australia: Inferences from landscape genetics analysis. *Journal of Applied Ecology*, 45, 1732–1741.
- Leckie, D. (1990). Advances in remote sensing technologies for forest survey and management. *Canadian Journal of Forest Research*, 21, 464–483.
- Leonard, T. D., Taylor, P. D., & Warkentin, I. G. (2008). Landscape structure and spatial scale affect space use by songbirds in naturally patchy and harvested boreal forests. *Condor*, 110, 467–481.
- Linke, J., Franklin, S. E., Hall-Beyer, M., & Stenhouse, G. (2008). Effects of cutline density and land-cover heterogeneity on landscape metrics in western Alberta. *Canadian Journal of Remote Sensing*, 34(4), 390–404.
- Linke, J., Franklin, S. E., Huettmann, F., & Stenhouse, G. (2005). Seismic cutlines, changing landscape metrics and grizzly bear landscape use in Alberta. *Landscape Ecology*, 20, 811–826.
- Linke, J., McDermid, G. J., Laskin, D. N., McLane, A. J., Pape, A., Cranston, J., et al. (in press). A disturbance-inventory framework for flexible and reliable landscape monitoring. *Photogrammetric Engineering and Remote Sensing*, 75(6).
- Linke, J., McDermid, G. J., Pape, A. D., McLane, A. J., Laskin, D. N., Hall-Beyer, M., et al. (2009). The influence of patch delineation mismatches on multi-temporal landscape pattern analysis. *Landscape Ecology*, 24(2), 157–170. doi:10.1007/s10980-008-9290-z
- Lunetta, R. S., Lyon, J. G., Guindon, B., & Elvidge, C. D. (1998). North American landscape characterization dataset development and fusion issues. *Photogrammetric Engineering & Remote Sensing*, 64, 821–829.
- Masek, J. G., & Collatz, G. J. (2006). Estimating forest carbon fluxes in a disturbed southeastern landscape: Integration of remote sensing, forest inventory, and biogeochemical modeling. *Journal of Geophysical Research—Biogeosciences*, 111.
- Masek, J. G., Huang, C. Q., Wolfe, R., Cohen, W., Hall, F., Kutler, J., et al. (2008). North American forest disturbance mapped from a decadal Landsat record. *Remote Sensing of Environment*, 112, 2914–2926.
- Masek, J. G., Vermote, E. F., Saleous, N. E., Wolfe, R., Hall, F. G., Huemmrich, K. F., et al. (2006). A Landsat surface reflectance dataset for North America, 1990–2000. *IEEE Geoscience and Remote Sensing Letters*, 3, 68–72.
- Mladenoff, D. J., White, M. A., Pastor, J., & Crow, T. R. (1993). Comparing spatial pattern in unaltered old-growth and disturbed forest landscapes. *Ecological Applications*, 3, 294–306.
- Moody, A., & Woodcock, C. E. (1994). Scale-dependent errors in the estimation of land-cover proportions - implications for global land-cover datasets. *Photogrammetric Engineering and Remote Sensing*, 60, 585–594.
- Morehouse, K., Johns, T., Kaye, J., & Kaye, A. (2008). Carbon and nitrogen cycling immediately following bark beetle outbreaks in southwestern ponderosa pine forests. *Forest Ecology and Management*, 255, 2698–2708.
- Morton, D. C., DeFries, R. S., Shimabukuro, Y. E., Anderson, L. O., Espirito-Santo, F. D. B., Hansen, M., et al. (2005). Rapid assessment of annual deforestation in the Brazilian Amazon using MODIS data. *Earth Interactions*, 9(Article number 8).
- Nielsen, S. E., Boyce, M. S., & Stenhouse, G. B. (2004). Grizzly bears and forestry I. Selection of clearcuts by grizzly bears in west-central Alberta, Canada. *Forest Ecology and Management*, 199, 51–65.
- Pape, A. D., & Franklin, S. E. (2008). MODIS-based change detection for Grizzly Bear habitat mapping in Alberta. *Photogrammetric Engineering and Remote Sensing*, 74, 973–985.
- Patenaude, G., Milne, R., & Dawson, T. P. (2005). Synthesis of remote sensing approaches for forest carbon estimation: Reporting to the Kyoto Protocol. *Environmental Science & Policy*, 8, 161–178.
- Price, J. (1994). How unique are spectral signatures? *Remote Sensing of Environment*, 49, 181–186.
- Potapov, P., Hansen, M. C., Stehman, S. V., Loveland, T. R., & Pittman, K. (2008). Combining MODIS and Landsat imagery to estimate and map boreal forest cover loss. *Remote Sensing of Environment*, 112, 3708–3719.
- Potter, C., Tan, P. N., Steinbach, M., Klooster, S., Kumar, V., Myneni, R., et al. (2003). Major disturbance events in terrestrial ecosystems detected using global satellite data sets. *Global Change Biology*, 9, 1005–1021.
- Ranson, K. J., Kovacs, K., Sun, G., & Kharuk, V. I. (2003). Disturbance recognition in the boreal forest using radar and Landsat-7. *Canadian Journal of Remote Sensing*, 29, 271–285.
- Roy, D., Ju, J., Lewis, P., Schaaf, C. B., Gao, F., Hansen, M. C., et al. (2008). Multi-temporal MODIS-Landsat data fusion for relative radiometric normalization, gap filling, and prediction of Landsat data. *Remote Sensing of Environment*, 112, 3112–3130.
- Seto, K. C., Woodcock, C. E., Song, C., Huang, X., Lu, J., & Kaufmann, R. K. (2002). Monitoring land-use change in the Pearl River Delta using Landsat TM. *International Journal of Remote Sensing*, 23, 1985–2004.
- Schimel, D. S., Emanuel, W., Rizzo, B., Smith, T., Woodward, F. I., Fisher, H., et al. (1997). Continental scale variability in ecosystem processes: Models, data, and the role of disturbance. *Ecological Monographs*, 67, 251–271.
- Slaymaker, D., Jones, K., Griffin, C., Finn, J., Scott, J., Tear, T., et al. (1996). Mapping deciduous forests in Southern New England using aerial videography and hyperclustered multi-temporal Landsat TM imagery. *Gap Analysis: A Landscape Approach to Biodiversity Planning*. (pp. 87–101). Bethesda, MD, USA: American Society of Photogrammetry and Remote Sensing.
- Spies, T. A., Ripley, W. J., & Bradshaw, G. A. (1994). Dynamics and pattern of a managed coniferous forest landscape in Oregon. *Ecological Applications*, 4, 555–568.
- Turner, M. G., Romme, W. H., Gardner, R. H., & Hargrove, W. W. (1997). Effects of fire size and pattern on early succession in Yellowstone National Park. *Ecological Monographs*, 67, 411–433.
- Vermote, E. F., & Kotchenova, S. Y. (2008). *MOD09 (Surface Reflectance) User's Guide, Version 1.1*. Website available at <http://modis-sr.ltdri.org> <<http://modis-sr.ltdri.org/>>
- Vermote, E. F., Tanre, D., Deuze, J. L., Herman, M., & Morcrette, J. J. (1997). Second Simulation of the Satellite Signal in the Solar Spectrum, 6S: An overview. *IEEE Transactions on Geoscience and Remote Sensing*, 35, 675–686.
- White, J. C., Coops, N. C., Hilker, T., Wulder, M. A., & Carroll, A. L. (2007). Detecting mountain pine beetle red attack damage with EO-1 Hyperion moisture indices. *International Journal of Remote Sensing*, 28, 2111–2121.
- Wu, J. D., Wang, D., & Bauer, M. E. (2005). Image-based atmospheric correction of QuickBird imagery of Minnesota cropland. *Remote Sensing of Environment*, 99, 315–325.
- Wulder, M. A., Dechka, J. A., Gillis, M. A., Luther, J. E., Hall, R. J., & Beaudoin, A. (2003). Operational mapping of the land cover of the forested area of Canada with Landsat data: EOSD land cover program. *Forestry Chronicle*, 79, 1075–1083.
- Wulder, M., & Dymond, C. (2003). *Remote sensing technologies for mountain pine beetle surveys*. In T. Shore, J. Brooks & J. Stone (Eds.). (pp. 146–153). Victoria, British Columbia: Natural Resources Canada, Canadian Forest Service, Pacific Forestry Centre.

- Wulder, M., Skakun, R., Kurz, W., & White, J. (2004). Estimating time since forest disturbance using segmented Landsat ETM+ imagery. *Remote Sensing of Environment*, 93, 179–187.
- Wulder, M. A., White, J. C., Goward, S. N., Masek, J. G., Irons, J. R., Herold, M., et al. (2008). Landsat continuity: Issues and opportunities for land cover monitoring. *Remote Sensing of Environment*, 112, 955–969.
- Zhan, X., Sohlberg, R. A., Townshend, J. R. G., DiMiceli, C., Carroll, M. L., Eastman, J. C., et al. (2002). Detection of land cover changes using MODIS 250 m data. *Remote Sensing of Environment*, 83, 336–350.
- Zhang, X., Freidl, M. A., Schaaf, C. B., Strahler, A. H., Hodges, J. C. F., Gao, F., et al. (2003). Monitoring vegetation phenology using MODIS. *Remote Sensing of Environment*, 84, 471–475.
- Zhang, X., Schaaf, C., Friedl, M. A., Strahler, A., Gao, F., & Hodges, J. (2002). MODIS Tasseled Cap transformation and its utility. In, *Geoscience and Remote Sensing Symposium, IGARSS '02. IEEE International*, 1063–1065.